

# Influence of triaxial deformation on wobbling motion in even-even nuclei

Bin Qi,<sup>1,\*</sup> Hui Zhang,<sup>1</sup> Shou Yu Wang,<sup>1</sup> and Qi Bo Chen<sup>2,†</sup>

<sup>1</sup>*Shandong Provincial Key Laboratory of Optical Astronomy and Solar-Terrestrial Environment,  
School of Space Science and Physics, Institute of Space Sciences,  
Shandong University, Weihai, 264209, People's Republic of China*

<sup>2</sup>*Physik-Department, Technische Universität München, D-85747 Garching, Germany*

The influence of triaxial deformation  $\gamma$  on the purely collective form of wobbling motion in even-even nuclei are discussed based on the triaxial rotor model. It is found that the harmonic approximation is realized well when  $\gamma = 30^\circ$  for the properties of energy spectra and electric quadrupole transition probabilities, while this approximation gets bad when  $\gamma$  deviates from  $30^\circ$ . A recent data from Coulomb excitation experiment, namely  $3_1^+$  and  $2_2^+$  for the  $^{110}\text{Ru}$  are studied and might be suggested as the bandhead of the wobbling bands. In addition, two types of angular momentum geometries for wobbling motion, stemming from different  $\gamma$  values, are exhibited by azimuthal plots.

## I. INTRODUCTION

Two unambiguous fingerprints of the stable triaxiality of nuclei are chirality [1] and wobbling [2], which have been studied actively over the past two decades. Wobbling motion was introduced by Bohr and Mottelson in 1970s [2]. It is described as small amplitude oscillation of the total angular momentum vector with respect to the principal axis with the largest moment of inertia. Since 2001, wobbling experimental evidence was first reported in  $^{163}\text{Lu}$  [3, 4], and later in  $^{161}\text{Lu}$ ,  $^{165}\text{Lu}$ ,  $^{167}\text{Lu}$ ,  $^{167}\text{Ta}$  nuclei [5–8]. In recent years, wobbling was reported in other regions as well:  $^{135}\text{Pr}$ ,  $^{133}\text{La}$  in the  $A \sim 130$  region [9–11],  $^{105}\text{Pd}$  in the  $A \sim 100$  region [12],  $^{187}\text{Au}$  and  $^{183}\text{Au}$  in the  $A \sim 190$  region [13, 14]. It is interesting to note that all of the aforementioned wobbling motions are in odd- $A$  nuclei.

For odd- $A$  nuclei, Frauendorf and Dönau showed two different possibilities of wobbling modes: longitudinal case and transverse case [15]. The theoretical descriptions of wobbling motion of odd- $A$  nucleus have been attracted great attention, and extensively studied with the triaxial particle rotor model (PRM) [15–19] and its approximation solutions [20–22], the random phase approximation [23–30], the angular momentum projection (AMP) methods [10, 31], or the collective Hamiltonian method [32, 33]. There are also some debates on the interpretations [15] for the wobbling in odd- $A$  nucleus [20, 34–36].

Meanwhile, wobbling modes in even-even nuclei [2] has been studied continuously in theory, e.g., see Refs. [37–44]. Recently, two new bands built on the two-quasiparticle  $\pi(h_{11/2})^2$  configuration were reported in even-even nuclei  $^{130}\text{Ba}$  [45], which were lately interpreted as the transverse wobbling bands by PRM [46] and AMP method [47]. However, one notes that the experimental evidence for the wobbling motion based on even-even nu-

cleus with zero quasi-particle configuration, namely the originally predicted purely collective form [2], is fragmentary yet. For instance, the possible evidence was pointed to the  $\gamma$ -band in  $^{112}\text{Ru}$  [48]. Unfortunately, there were not interband  $\gamma$  rays connecting between the candidates of wobbling band.

The recent advent of new-generation detectors has been opening a great possibility to explore a new area of the collective rotation physics, in which one interesting exploration is searching for the wobbling mode with purely collective form. Prior to this, the investigation for the variation of the wobbling excited bands with respect to the triaxial parameter  $\gamma$  could be helpful for the experimental exploration. In addition, a clear picture of the angular momentum geometry and its evolution for the wobbling excitation with purely collective form will also be helpful to better understand the wobbling phenomena in odd- $A$  nuclei. Motivated by the above considerations, in this paper we discuss systematically the wobbling excitation in even-even nuclei using triaxial rotor model.

## II. DISCUSSION

### A. Influence of $\gamma$ value on the harmonic approximation

The moment of inertia (MoI) is a key parameter to describe the wobbling excitation. The hydrodynamical MoI is very reasonable for the triaxial deformed nuclei, and is consistent with cranking shell model [34]. In Fig. 1(a), we present the hydrodynamical MoI of the three principal axes [49],

$$\mathcal{J}_k = \mathcal{J}_0 \sin^2\left(\gamma - \frac{2}{3}\pi k\right), \quad (1)$$

with  $\gamma$  the triaxial deformation parameter and the unit of  $\mathcal{J}_0$ . In the range of  $0 \leq \gamma \leq \pi/3$ ,  $k = 1, 2, 3$  corresponds to the intermediate ( $m$ -), short ( $s$ -) and long ( $l$ -) axis, respectively. Obviously,  $\mathcal{J}_1$ , i.e., the MoI of the  $m$ -axis, is the largest.

The harmonic approximation (HA) for the wobbling excitation and the theoretical framework of triaxial ro-

\*Electronic address: bqi@sdu.edu.cn

†Electronic address: qbchen@pku.edu.cn

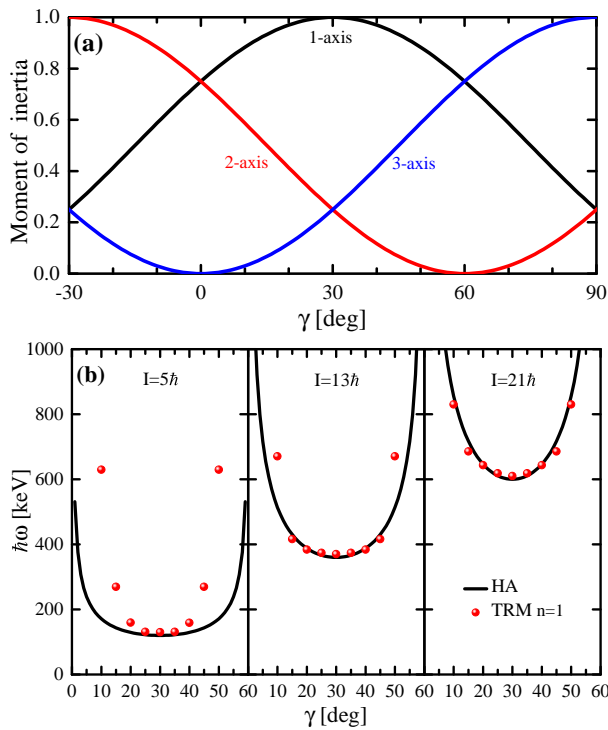


FIG. 1: (a) The hydrodynamical MoI of the three principal axes (denoted by  $k = 1, 2, 3$ ) as functions of  $\gamma$ . The unit is taken as  $\mathcal{J}_0$ . (b) The wobbling frequency as functions of the  $\gamma$  calculated by HA formula Eq. (2) and TRM using Eq. (5) with  $n = 1$ .

tor model (TRM) can be found in Ref. [2]. Using the hydrodynamical MoI, the wobbling frequency calculated by HA formula

$$\hbar\omega = I \left[ \left( \frac{1}{\mathcal{J}_2} - \frac{1}{\mathcal{J}_1} \right) \left( \frac{1}{\mathcal{J}_3} - \frac{1}{\mathcal{J}_1} \right) \right]^{1/2}, \quad (2)$$

as functions of the  $\gamma$  for  $I = 5, 13, 21\hbar$  are shown in Fig. 1(b). Here, we take a value of  $\mathcal{J}_0 = 100 \hbar^2 \text{MeV}^{-1}$ , which is slightly larger than  $\sim 70 \hbar^2 \text{MeV}^{-1}$  in  $^{163}\text{Lu}$  [15]. The wobbling frequency is the smallest at  $\gamma = 30^\circ$ , and increases as the  $\gamma$  deviates from  $30^\circ$ . It increases dramatically for  $\gamma < 10^\circ$  or  $\gamma > 50^\circ$ . The  $\hbar\omega$  value is direct proportion to  $1/\mathcal{J}_0$ . Thus, if  $\mathcal{J}_0$  takes value of  $20 \hbar^2 \text{MeV}^{-1}$  (suitable for  $^{135}\text{Pr}$  [15]),  $\hbar\omega$  will be five times as large as these values in Fig. 1(b).

For comparison, the  $\hbar\omega$  extracted from TRM are also shown, and the  $\hbar\omega$  in HA becomes better in agreement with the frequency extracted from TRM when  $\gamma$  is closer to  $30^\circ$  and spin is larger.

As shown in Fig. 1(b), the  $\gamma$  degree of freedom is very important in determining the properties of triaxial nuclei. To examine the quality of HA, we calculate the results of all  $\gamma$  values systematically in the TRM. As is known, the nucleus described as  $(\beta_2, \gamma)$  have the identical shape with  $(\beta_2, -\gamma)$ ,  $(\beta_2, \pm\gamma \pm 120^\circ)$ , where  $\beta_2$  is the quadruple deformation. Thus only the results in the  $\gamma$  ranging from  $0^\circ$  to  $60^\circ$  are sufficient for discussion. Moreover, due to

the symmetry of  $\mathcal{J}_k$  with respect to  $\gamma = 30^\circ$  as shown in Fig. 1, the results for  $30^\circ + \Delta\gamma$  ( $55^\circ$  to  $35^\circ$ ) are identical to the corresponding results for  $30^\circ - \Delta\gamma$  ( $5^\circ$  to  $25^\circ$ ). Thus we can only focus on the results for  $\gamma$  from  $0^\circ$  to  $30^\circ$ .

The energy spectra, wobbling energies, as well as the reduced electric quadrupole transition probabilities as functions of spin for the several lowest bands calculated by TRM for  $\gamma$  changing from  $5^\circ$  to  $25^\circ$  are shown in Fig. 2 and for  $\gamma = 30^\circ$  in Fig. 3, in comparison with those obtained by the HA formulas. The energy spectra are obtained by diagonalizing the TRM Hamiltonian [2],

$$\hat{H} = \sum_{k=1}^3 \frac{\hat{I}_k^2}{2\mathcal{J}_k} = A_1 \hat{I}_1^2 + A_2 \hat{I}_2^2 + A_3 \hat{I}_3^2, \quad (3)$$

with  $A_k = 1/(2\mathcal{J}_k)$ . The wobbling energies, defined as the energy differences between the excited states and the yrast state, are extracted as [43]

$$E_{\text{wob}} = E(n, I) - E(0, I), \quad (4)$$

for even  $n$  bands, and

$$E_{\text{wob}} = E(n, I) - \frac{1}{2}[E(0, I-1) + E(0, I+1)], \quad (5)$$

for odd  $n$  bands, in which  $E(n, I)$  denotes the energy of spin  $I$  in the  $n$ -th excited band. The reduced electromagnetic transition probabilities are calculated by the operator [2]

$$\hat{\mathcal{M}}(E2, \mu) = \sqrt{\frac{5}{16\pi}} \hat{Q}_{2\mu}, \quad (6)$$

with the obtained eigen TRM wave functions. The quadrupole moments in the laboratory frame ( $\hat{Q}_{2\mu}$ ) and the intrinsic system ( $\hat{Q}'_{2\mu}$ ) are connected by the relation

$$\begin{aligned} \hat{Q}_{2\mu} &= \mathcal{D}_{\mu 0}^{2*} \hat{Q}'_{20} + (\mathcal{D}_{\mu 2}^{2*} + \mathcal{D}_{\mu -2}^{2*}) \hat{Q}'_{22} \\ &= \mathcal{D}_{\mu 0}^{2*} Q \cos \gamma + (\mathcal{D}_{\mu 2}^{2*} + \mathcal{D}_{\mu -2}^{2*}) \frac{1}{\sqrt{2}} Q \sin \gamma. \end{aligned} \quad (7)$$

For small triaxial deformation  $\gamma = 5^\circ$  and  $10^\circ$ , there is rather large difference between the HA and TRM results. For  $\gamma = 15^\circ$ , the wobbling energies for  $I > 10\hbar$  of  $n = 1$  band in HA are in agreement with those in TRM, while for  $n > 1$  bands in HA have large deviation from TRM results. As the  $\gamma$  increasing, the quality of agreement between TRM and HA becomes better. HA results for both energy spectra and wobbling energies are in nice agreement with TRM over the whole spin range for small  $n=1, 2$  phonon wobbling bands for  $\gamma = 25^\circ$ . When  $\gamma = 30^\circ$ , the HA formulas could give very good descriptions for the TRM results, which implies that the rotational axis exhibit a very good harmonic oscillations with respect to  $m$ -axis with the largest MoI.

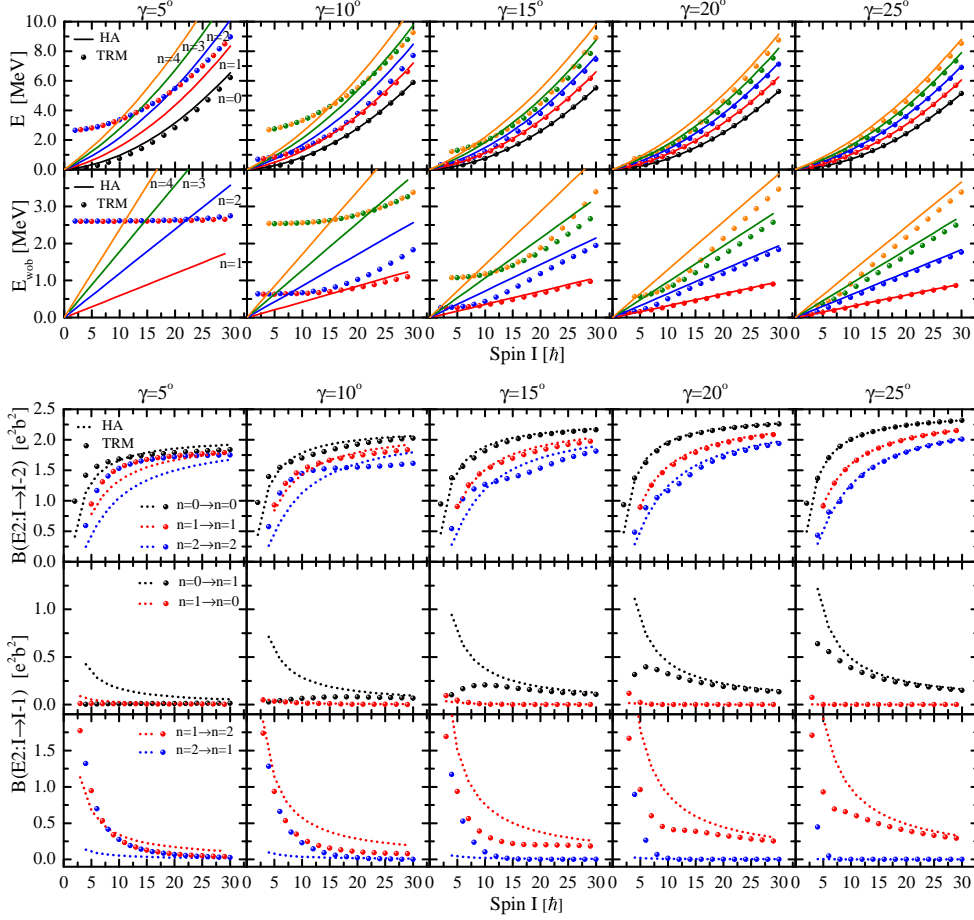


FIG. 2: Upper panels: The energy spectra and wobbling energies for several lowest bands calculated by TRM (dots) compare with those by HA formulas (lines) for  $\gamma$  changing from  $5^\circ$  to  $25^\circ$ . Lower panels: The intraband and interband  $B(E2)$  values for  $n = 0, 1$ , and  $2$  bands calculated by TRM compare with those by HA formulas.

The intraband and interband  $B(E2)$  in HA formulas are calculated as [2]:

$$B(E2; nI \rightarrow n, I \pm 2) \approx \frac{5}{16\pi} e^2 Q_2^2 \quad (8)$$

$$B(E2; nI \rightarrow n-1, I-1) = \frac{5}{16\pi} e^2 \frac{n}{I} \left( \sqrt{3}Q_0x - \sqrt{2}Q_2y \right)^2 \quad (9)$$

$$B(E2; nI \rightarrow n+1, I-1) = \frac{5}{16\pi} e^2 \frac{n+1}{I} \left( \sqrt{3}Q_0y - \sqrt{2}Q_2x \right)^2, \quad (10)$$

where  $Q_0$  and  $Q_2$  are the quadrupole moments with respect to the  $m$ -axis, and  $x = \sqrt{[\alpha/(\hbar\omega) + 1]/2}$ ,  $y = \sqrt{[\alpha/(\hbar\omega) - 1]/2}$  with  $\alpha \equiv (A_2 + A_3 - 2A_1)I$ . The quadrupole moment  $Q = \sqrt{e^2Q_0^2 + e^2Q_2^2}$  takes values of  $\sqrt{16\pi}$  eb in the calculations, which is close to the value of  $\sim 9$  eb in Lu isotopes [3].

For the intraband  $B(E2, I \rightarrow I-2)$  values, the HA results given by Eq. (8) are constants, which are independent of spin  $I$  and wobbling phonon number. This equation results from the approximation of  $\langle I, K, 2, -2 | I -$

$2, K' \rangle \approx 1$  [2]. Here, we restore the approximation by adding the square of CG coefficient  $\langle I, K, 2, -2 | I - 2, K' \rangle^2$ , with  $K = I - n$ ,  $K' = I - 2 - n$ . The values of  $K$  and  $K'$  are taken based on the wobbling picture with  $\gamma = 30^\circ$ . A similar recipe for  $n = 0, 1$  bands was already made in Ref. [18]. After such modifications, the HA formula could describe well the characteristics of TRM results, which show the increasing trend of intraband  $B(E2)$  as the increase of wobbling phonon number.

For interband  $B(E2, I \rightarrow I-1)$  values, the HA results exhibit a decreasing trend with respect to spin, which are determined by the factor  $1/I$  in the HA formulas Eqs. (9) and (10). The  $B(E2; n, I \rightarrow n-1, I-1)$  are very small over almost the whole spin region. For each  $\gamma$  under our discussion, the strength of the interband  $B(E2; n, I \rightarrow n+1, I-1)$  is smaller than that of the intraband  $B(E2; n, I \rightarrow n, I-2)$  in the high spin region by a factor of order  $n/I$  [2]. Again, the agreement between HA values and TRM results becomes better as the increase of  $\gamma$ .

From both the comparisons of the energy spectra and electric quadrupole transition probabilities of the HA and

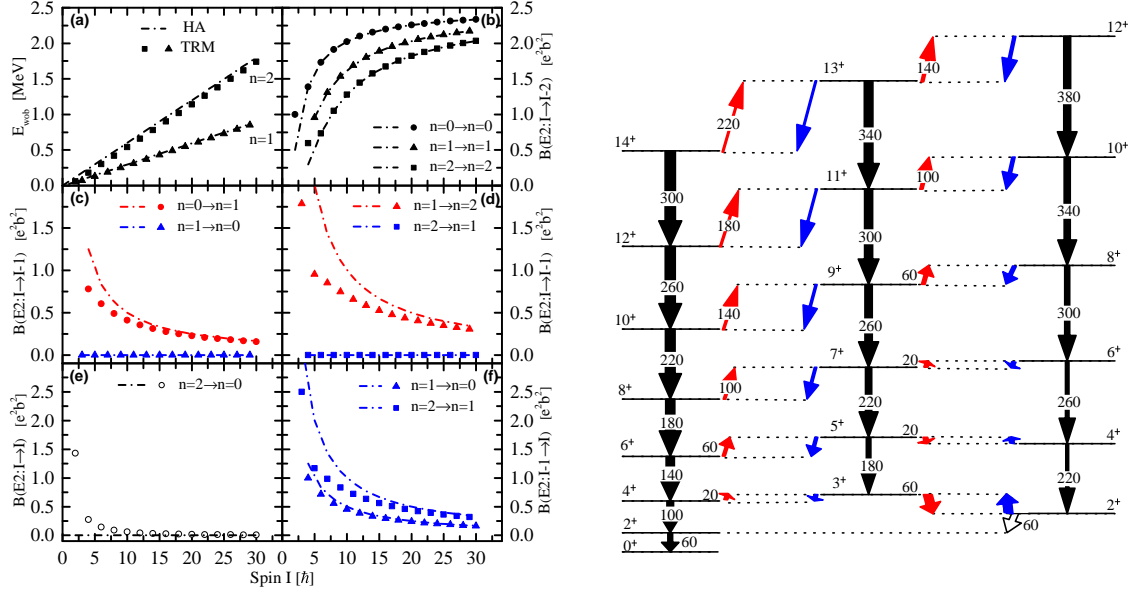


FIG. 3: Left panels: The wobbling energies, the intraband and interband  $B(E2)$  values for the ground band and  $n = 1, 2$  wobbling bands calculated by TRM with  $\gamma = 30^\circ$  compare with those in HA. Right panels: The energy level scheme calculated by the TRM for the ground band and  $n = 1, 2$  wobbling bands. The transition energy are denoted, and the thickness of the transitions is proportional to  $B(E2)$  values.

TRM, it is found that the agreement are very nice for  $\gamma$  changing from  $\sim 25^\circ$  to  $\sim 35^\circ$  over the whole spin range for  $n=0, 1$ , and  $2$  bands.

### B. $K_m$ of wobbling motion

The above discussion to judge the quality of HA is based on the observable of energy and electric quadrupole transition probability. We further analyze the information of angular momentum to understand this question. For this purpose, the root mean square of projection of total angular momentum along the  $m$ -axis, namely  $\langle K_m^2 \rangle^{1/2}$  are calculated in TRM as

$$\begin{aligned} \langle K_m^2 \rangle^{1/2} &= \langle IM | \hat{I}_1^2 | IM \rangle^{1/2} \\ &= \langle IM | (\hat{I}_+ + \hat{I}_-)^2 / 4 | IM \rangle^{1/2}. \end{aligned} \quad (11)$$

Here, the  $|IM\rangle$  is the eigen wave function of TRM,

$$|IM\rangle = \sum_{K \geq 0} C_{IK} |IMK+\rangle, \quad (12)$$

expanded on the basis

$$|IMK+\rangle = \sqrt{\frac{2I+1}{16\pi^2(1+\delta_{K0})}} [\mathcal{D}_{MK}^I + (-1)^I \mathcal{D}_{M-K}^I]. \quad (13)$$

The root mean square of  $K_m$  with  $\gamma$  changing from  $5^\circ$  to  $30^\circ$  for  $I = 4, 5, 12, 13, 20, 21\hbar$  are shown in Fig. 4.

It is found that the relationship  $\langle K_m^2 \rangle^{1/2} = I - n$  with  $n = 1, \dots, n_{\text{max}}$  are satisfied strictly for  $\gamma = 30^\circ$ . The differences  $\langle K_m^2 \rangle^{1/2}$  and  $I - n$  will increase if  $\gamma$  gradually deviates from  $30^\circ$ , or if the phonon number  $n$  gradually increases.

The above variation as  $\gamma$  and  $n$  can be understood by the  $K_m$  structure, namely the probability distribution of different  $K_m$  values. As examples, the  $K_m$  structure for all states with different phonon number at spin  $12\hbar$  and  $13\hbar$  are shown in Table I.

Let us first investigate the case of  $\gamma = 30^\circ$ . It is much easier to express the results from  $\gamma = 90^\circ$ , which has the identical shape with  $\gamma = 30^\circ$  except the  $m$ -axis is chosen as the quantum 3-axis. Due to  $\mathcal{J}_1 = \mathcal{J}_2$ ,  $A_1 = A_2 = 4A_3$  in Eq. (3) when  $\gamma = 90^\circ$ , the Hamiltonian reads now

$$\hat{H} = \frac{1}{2}(A_1 + A_2)(\hat{I}^2 - \hat{I}_3^2) + A_3 \hat{I}_3^2. \quad (14)$$

Thus the projection  $K_m$  is good quantum number. From the calculated results the following relationship are satisfied strictly for  $n = 1, \dots, n_{\text{max}}$ ,

$$K_m = I - n. \quad (15)$$

When  $\gamma$  deviates from  $\gamma = 30^\circ$ , the non-diagonal term in Eq. (3) will introduce the  $K$ -mixing,  $K_m$  is not a good quantum number. As shown in Table I, for  $n = 0$  ground state of  $12\hbar$ , the components of  $K_m = 12$  is over 90% when  $\gamma = 25^\circ$  and  $20^\circ$ , and decreases to 76% when  $\gamma = 15^\circ$ . For  $n = 2$  phonon state, the component of  $K_m = I - 2 = 10$  is the dominant one for  $\gamma = 25^\circ$ .

TABLE I:  $K_m$ -structure for  $I = 12$  and  $13\hbar$ 

$I = 12\hbar$	$\gamma = 30^\circ$	$\gamma = 25^\circ$	$\gamma = 20^\circ$	$\gamma = 15^\circ$
n=0	100% 12⟩	98% 12⟩ + 2% 10⟩	90% 12⟩ + 8% 10⟩ + 1% 8⟩	76% 12⟩ + 15% 10⟩ + 5% 8⟩
n=2	100% 10⟩	81% 10⟩ + 15% 8⟩ + 2% 12⟩	35% 10⟩ + 29% 8⟩ + 15% 6⟩	21% 2⟩ + 20% 4⟩ + 19% 6⟩
n=4	100% 8⟩	38% 8⟩ + 31% 6⟩ + 13% 10⟩	29% 2⟩ + 26% 10⟩ + 20% 4⟩	33% 10⟩ + 19% 2⟩ + 19% 8⟩
n=6	100% 6⟩	35% 2⟩ + 24% 8⟩ + 20% 4⟩	25% 10⟩ + 23% 6⟩ + 21% 8⟩	37% 10⟩ + 28% 6⟩ + 13% 0⟩
n=8	100% 4⟩	37% 6⟩ + 21% 8⟩ + 20% 0⟩	39% 8⟩ + 23% 4⟩ + 15% 0⟩	43% 8⟩ + 26% 4⟩ + 14% 0⟩
n=10	100% 2⟩	47% 4⟩ + 29% 6⟩ + 21% 0⟩	39% 6⟩ + 33% 4⟩ + 18% 0⟩	41% 6⟩ + 28% 4⟩ + 17% 0⟩
n=12	100% 0⟩	48% 2⟩ + 38% 0⟩ + 12% 4⟩	48% 2⟩ + 34% 0⟩ + 16% 4⟩	47% 2⟩ + 33% 0⟩ + 17% 4⟩
$I = 13\hbar$	$\gamma = 30^\circ$	$\gamma = 25^\circ$	$\gamma = 20^\circ$	$\gamma = 15^\circ$
n=1	100% 12⟩	93% 12⟩ + 7% 10⟩	72% 12⟩ + 21% 10⟩ + 5% 8⟩	47% 12⟩ + 29% 10⟩ + 15% 8⟩
n=3	100% 10⟩	66% 10⟩ + 23% 8⟩ + 7% 12⟩	31% 8⟩ + 22% 6⟩ + 20% 12⟩	35% 12⟩ + 25% 6⟩ + 17% 8⟩
n=5	100% 8⟩	36% 6⟩ + 24% 8⟩ + 21% 10⟩	37% 10⟩ + 27% 4⟩ + 16% 6⟩	34% 10⟩ + 23% 4⟩ + 15% 12⟩
n=7	100% 6⟩	37% 8⟩ + 35% 4⟩ + 19% 2⟩	32% 8⟩ + 23% 10⟩ + 22% 2⟩	31% 10⟩ + 23% 8⟩ + 22% 2⟩
n=9	100% 4⟩	46% 6⟩ + 36% 2⟩ + 14% 8⟩	37% 6⟩ + 31% 2⟩ + 28% 8⟩	33% 8⟩ + 31% 6⟩ + 29% 2⟩
n=11	100% 2⟩	46% 4⟩ + 42% 2⟩ + 12% 6⟩	47% 4⟩ + 33% 2⟩ + 18% 6⟩	46% 4⟩ + 30% 2⟩ + 21% 6⟩

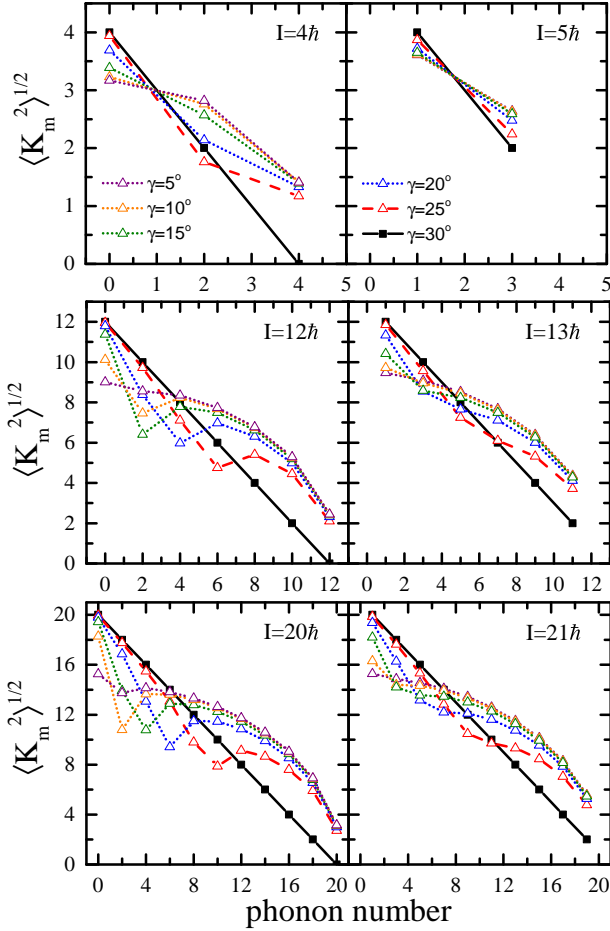


FIG. 4: The root mean square of the projections of total angular momentum on the  $m$ -axis ( $K_m$ ) with  $\gamma$  changing from  $5^\circ$  to  $30^\circ$  for  $I = 4, 5, 12, 13, 20, 21\hbar$ .

Here, we think the probability of the  $K_m = I - n$  component larger than 50% might be chosen as a reasonable criteria to judge the quality of HA approximation. Based on this suggested criteria, wobbling bands are re-

alized perfectly for  $\gamma = 30^\circ$ . For spin  $12\hbar$  and  $13\hbar$ , nice wobbling occurs for  $n = 1, 2, 3$  phonon excitation when  $\gamma = 25^\circ$ , and for  $n = 1$  phonon excitation when  $\gamma = 20^\circ$ . As the spin increasing, the HA wobbling approximation becomes better. For the states of  $20\hbar$  and  $21\hbar$ , the probability of  $K_m = I - n$  larger than 50% is  $n = 1, 2, 3, 4$  phonon excitation when  $\gamma = 25^\circ$ . The obtained conclusion to judge the quality of HA from the probability of the  $K_m = I - n$  component is very consistent with those judgements from the energy and transition.

### C. Level scheme of wobbling band with $\gamma = 30^\circ$

According to the above discussion, the stable large triaxial deformation is necessary for the realization of the wobbling excitation. For the realistic even-even nuclei, the stable triaxial deformation is rare in the ground state [50]. A stable rigid triaxial deformation with  $\gamma \in (25^\circ, 35^\circ)$  is indeed a relatively strict condition. It might be one reason why the purely collective form was difficult to be observed in experiment in the past decades.

We would further explore level scheme for  $\gamma = 30^\circ$ , which shows a very good wobbling picture, with the hypothesis of a stable rigid triaxial deformation. Bohr and Mottelson discussed the excited energies of  $\gamma = 30^\circ$  very briefly in appendix 6B of textbook [2]. In Fig. 3, the wobbling energies and the  $B(E2)$  values for the two lowest wobbling bands calculated by TRM with  $\gamma = 30^\circ$  are shown in comparison with those from the HA formulas. The HA formulas in panel (e) and (f) are new deduced in this paper according to the method in the textbook [2] as

$$B(E2; n, I \rightarrow n - 2, I) \approx \frac{5}{16\pi} e^2 Q_0^2 \quad (16)$$

$$B(E2; n, I - 1 \rightarrow n - 1, I) \approx \frac{5}{16\pi} e^2 \frac{n}{I} \left( \sqrt{3} Q_0 y - \sqrt{2} Q_2 x \right)^2. \quad (17)$$

In the right panel, we show level scheme from the TRM

results of the ground band and the  $n = 1$  and 2 wobbling bands. The values of transition energies are marked, and the thickness of the transition is proportional to  $B(E2)$  values.

From the level scheme, some interesting relationships are exhibited as follows,

1.  $E(0, I + 2) - E(0, I) = E(1, I + 5) - E(0, I + 6) = E(2, I + 8) - E(1, I + 9)$ , e.g., 60 keV is the transition energy for  $(0, 2) \rightarrow (0, 0)$ ,  $(1, 5) \rightarrow (0, 6)$  and  $(2, 8) \rightarrow (1, 9)$ . Similar for 100 keV and 140 keV.
2.  $E(0, I + 2) - E(0, I) = E(1, I - 1) - E(1, I - 3) = E(2, I - 4) - E(2, I - 6)$ , e.g., 220 keV is the transition energy for  $(0, 10) \rightarrow (0, 8)$ ,  $(1, 7) \rightarrow (1, 5)$  and  $(2, 4) \rightarrow (2, 2)$ . Similar for 260 keV and 300 keV.
3.  $[E(n, I + 4) - E(n, I + 2)] - [E(n, I + 2) - E(n, I)] = 40$  keV.

These relationships are understood as follows. From the Hamiltonian of TRM in Eq. (14), one obtains

$$E(n, I) = A_3 I(I + 1) + 6A_3 I(n + \frac{1}{2}) - 3A_3 n^2. \quad (18)$$

Alternatively, from the HA formula ( $A_1 = A_2 = 4A_3$ ) with  $\hbar\omega = 2I\sqrt{(A_2 - A_3)(A_1 - A_3)} = 6IA_3$ , one obtains

$$E(n, I) = A_3 I(I + 1) + 6A_3 I(n + \frac{1}{2}). \quad (19)$$

Therefore, from either Eq. (18) or Eq. (19), one gets

$$E(n, I + 2) - E(n, I) = 4A_3(I + 3n) + 12A_3, \quad (20)$$

and thus the above relationships 2 and 3. Furthermore, from Eq. (18), one gets

$$E(n + 1, I + 5) - E(n, I + 6) = 4A_3(I - 3n) + 12A_3 \quad (21)$$

and thus relationship 1. Note that the HA formula Eq. (19) can not derive the relationship 1 due to the lack of  $-3A_3 n^2$  term. In addition, each values of energy in the level scheme will change according to the rule of  $1/\mathcal{J}_0$  for different  $\mathcal{J}_0$ .

There are one interesting thing worthwhile to be noted from Fig. 2 and Fig. 3(c), (d), the interband  $B(E2, I \rightarrow I - 1)$  for  $n = 1 \rightarrow n = 0$  and  $n = 2 \rightarrow n = 1$  are strongly suppressed for both HA and TRM results. Similar conclusions were obtained in Refs. [42]. In the observed wobbling bands in odd- $A$  nuclei, the interband  $B(E2, I \rightarrow I - 1)$  exists and links the wobbling excited band and yrast band, e.g. see Refs. [4, 9]. It could be inferred that the linking transitions between the wobbling bands of even-even nuclei are different from those in odd- $A$  nuclei.

As shown in the level scheme in Fig. 3, the  $B(E2, I \rightarrow I - 1)$  from  $n = 0$  to  $n = 1$  wobbling band will not occur spontaneously due to it needs to absorb energy. Such transitions are suggested to be realized by the method of Coulomb excitation, which has explored the transitions at the lower spin region of triaxial or octupole deformed nuclei recently [53, 54].

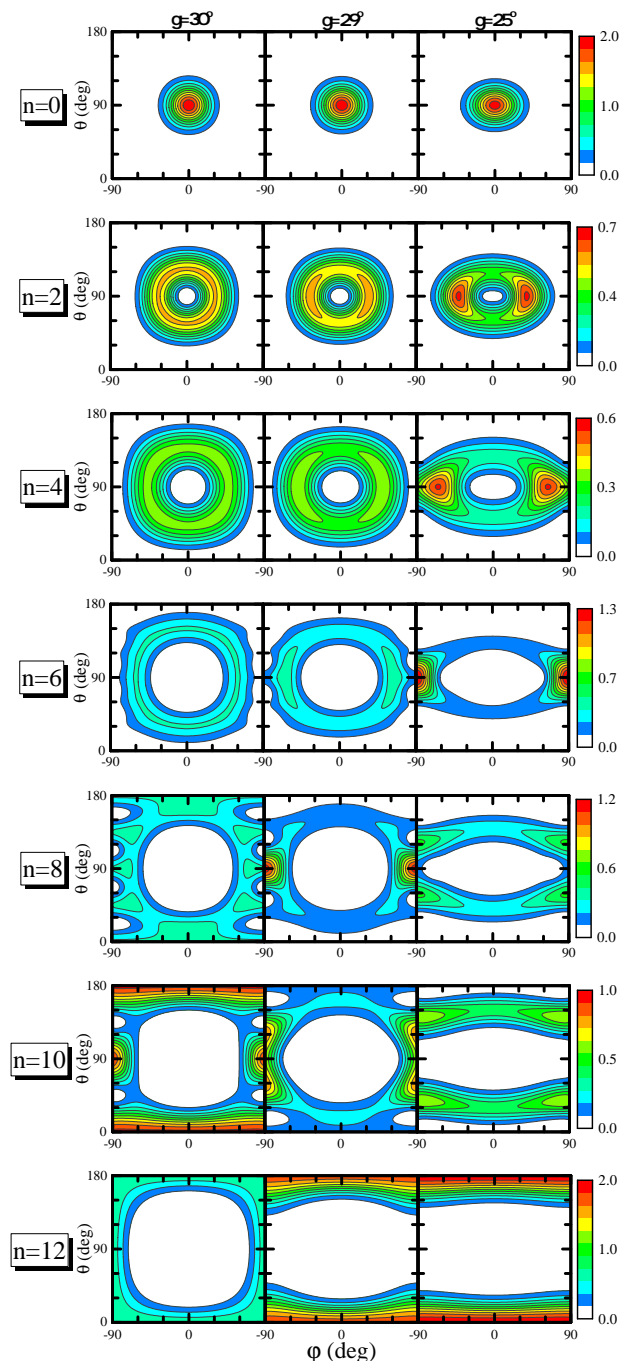


FIG. 5: Azimuthal plots for states with phonon number  $n = 0, 2, 4, 6, 8, 10,$  and  $12$  at  $I = 12\hbar$  calculated by TRM with  $\gamma = 30^\circ, 29^\circ,$  and  $25^\circ$ .

#### D. Two types of angular momentum geometries

In this work, we want to illustrate the angular momentum geometry of the wobbling motion by a probability density profile on the  $(\theta, \varphi)$  unit sphere, called azimuthal plot [19, 51, 52]. Here,  $(\theta, \varphi)$  are the orientation angles of the angular momentum vector  $\mathbf{I}$  (expectation value with  $M = I$ ) with respect to the intrinsic frame. The polar

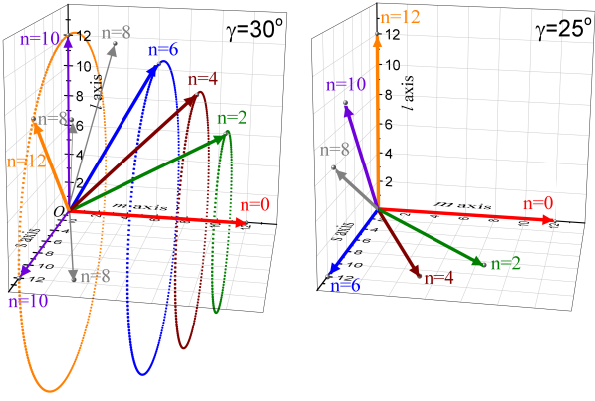


FIG. 6: Schematic illustration of angular momentum geometry at spin  $I = 12\hbar$  for  $\gamma = 30^\circ$  and  $\gamma = 25^\circ$ . The orientation of arrows refer to the maxima in the azimuthal plots in Fig. 5.

angle  $\theta$  is the angle between  $\mathbf{I}$  and the  $l$ -axis, whereas the azimuthal angle  $\varphi$  is the angle between the projection of  $\mathbf{I}$  on the  $m$ - $s$  plane and the  $m$ -axis. The profile can be obtained by relating the orientation angles  $(\theta, \varphi)$  to the Euler angles  $(\psi, \theta, \pi - \varphi)$ , where the  $z$  axis in the laboratory frame is chosen along  $\mathbf{I}$ . The profile is calculated as [19, 52]

$$\begin{aligned} \mathcal{P}^{(\nu)}(\theta, \varphi) &= \langle I, \theta \varphi | II\nu \rangle^2 \\ &= \sum_{KK'} D_{KI}^{I*}(\theta, \varphi, 0) C_{IK}^{(\nu)} C_{IK'}^{(\nu)} D_{K'I}^I(\theta, \varphi, 0), \end{aligned} \quad (22)$$

where  $C_{IK}^{(\nu)}$  are the expansion coefficients in Eq. (12).

In Fig. 5, the obtained profiles  $\mathcal{P}(\theta, \varphi)$  are shown for the ground state and all of the wobbling excited states at spin  $12\hbar$ . To visualize the results of Fig. 5, we show the schematic of angular momenta geometry in Fig. 6. Note that the orientation of the angular momentum vector in this figure just corresponds to the position of the maxima of  $\mathcal{P}(\theta, \varphi)$ . We choose three results for  $\gamma = 30^\circ, 29^\circ$  and  $25^\circ$ , whose ratio of  $\mathcal{J}_m : \mathcal{J}_s : \mathcal{J}_l$  are 4 : 1 : 1, 4.3 : 1.1 : 1 and 5.6 : 1.8 : 1, respectively.

One observes that the maximum of  $\mathcal{P}(\theta, \varphi)$  is always located at  $\theta = 90^\circ, \varphi = 0^\circ$  for the ground state, which means along the  $m$ -axis. The excited states exhibit different features for different  $\gamma$  values.

For  $\gamma = 25^\circ$  in the right panels of Fig. 5,  $\mathcal{P}(\theta, \varphi)$  show a very clear evolution of the angular momentum as the increase in the phonon number:  $m$ -axis ( $n = 0$ )  $\rightarrow$   $m$ - $s$  plane ( $n = 2, 4$ )  $\rightarrow$   $s$ -axis ( $n = 6$ )  $\rightarrow$   $s$ - $l$  plane ( $n = 8, 10$ )  $\rightarrow$   $l$ -axis ( $n = 12$ ). This process are also shown in Fig. 6. In some previous discussions, e.g., Ref. [15, 43], similar picture was mentioned based on the case of  $\mathcal{J}_m : \mathcal{J}_s : \mathcal{J}_l = 6 : 2 : 1$ .

The picture of  $\gamma = 30^\circ$  is different from that of  $25^\circ$ . The  $\mathcal{P}(\theta, \varphi)$  is cylindrical symmetry with ( $\theta = 90^\circ, \varphi = 0^\circ$ ) since  $\mathcal{J}_s = \mathcal{J}_l$ . One notes that since the length of  $s$ - and  $l$ - axis are different, such precessional motion of

rotational axis with respect to  $m$ -axis still makes sense. For  $n = 2, 4, 6$  states, the largest probability of angular momentum has the radius of the circle about  $30^\circ, 45^\circ$  and  $60^\circ$ , respectively, indicating the amplitude of fluctuation of the rotation axis is getting larger. The orientation of angular momentum with the largest probability are also shown in dotted line in Fig. 6.

The results of  $\gamma = 29^\circ$  is mixture of the character between  $\gamma = 30^\circ$  and  $25^\circ$  cases.  $n = 2$  state of  $29^\circ$  is close to the case of  $30^\circ$ , while  $n = 12$  state of  $29^\circ$  is close to the case of  $25^\circ$ .

Furthermore, the azimuthal plots and the schematic of angular momenta for the band of  $n = 0, 1, 2$  with the increase of spin are shown in Fig. 7. One observes that the angle between angular momentum and  $m$ -axis decreases as the spin increasing, for both  $n = 1$  and  $n = 2$  wobbling bands, which is consistent with the HA formula with the precession amplitude  $\sqrt{n/I}$ .

### E. Comparison with the recent data of $^{110}\text{Ru}$

Recently, a multi-step Coulomb excitation measurement was carried out for  $^{110}\text{Ru}$  isotope [54]. The experimental data of  $^{110}\text{Ru}$  are shown in Fig. 8(b), where the excitation energies (in keV) and spin-parity values are given above the states. The widths and labels of the arrows represent the measured reduced  $E2$  transition probabilities in W.u.. It should be noted the  $2_2^+$  and  $3_1^+$  are considered as one band in the Ref. [54], while we separate them in the present level schemes. Ref. [54] pointed out that the data provides direct evidence of relatively rigid triaxial deformation near the ground state.

In Fig. 8(a) and (c), we show the results calculated by TRM with  $\gamma = 30^\circ$  and  $25^\circ$ . The adopted parameter of MoI  $\mathcal{J}_0$  ( $\sim 24 \hbar^2 \text{MeV}^{-1}$ ) and quadruple moment  $Q$  ( $\sim 3.3 \text{ eb}$ ) are adjusted for the energy and  $B(E2)$  value of  $2_1^+$  state.

The calculated results are in agreement with the experimental data qualitatively. As mentioned and emphasized in Ref. [54], the relatively large  $2_2^+ \rightarrow 2_1^+$  and small  $2_2^+ \rightarrow 0_1^+$  matrix elements, are strong indications of triaxial deformation. These experimental characteristics are reproduced by the present calculations. In addition, the large  $3_1^+ \rightarrow 2_2^+$  and small  $3_1^+ \rightarrow 2_1^+$  matrix elements in experiment are reproduced by TRM. Based on this,  $3_1^+$  and  $2_2^+$  for the  $^{110}\text{Ru}$  might be suggested as the bandhead of the one- and two-phonon wobbling bands.

## III. SUMMARY

The influence of triaxial parameter  $\gamma$  on the wobbling excitation in even-even nuclei are investigated using the TRM with the hydrodynamical MoIs. We suggest that the probability of the  $K_m = I - n$  component larger than 50% might be a reasonable criteria to judge the quality HA. Based on this criteria and the characteristic of the

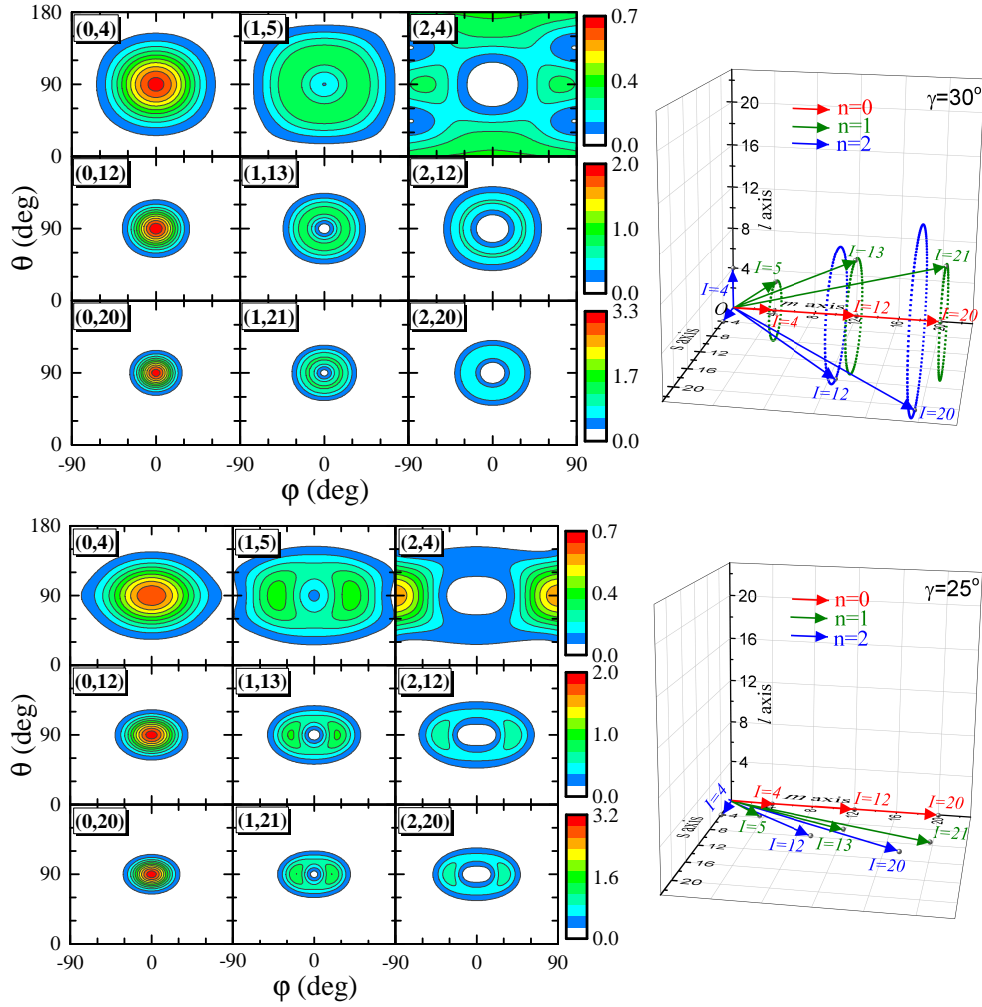


FIG. 7: Azimuthal plots for states  $(n, I)$ , in which  $I = 4, 5, 12, 13, 20, 21\hbar$  with  $n = 0, 1, 2$ , and the schematic illustration of the evolution of angular momenta for the wobbling band. Results for  $\gamma = 30^\circ$  and  $25^\circ$  are shown in upper and lower panels, respectively.

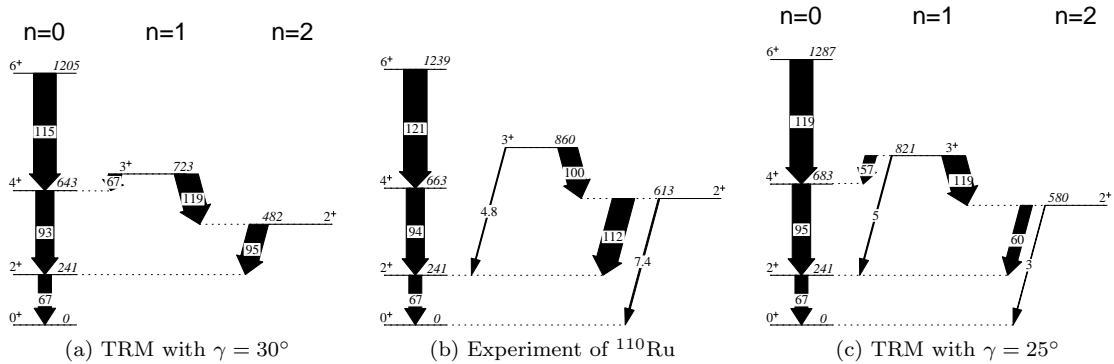


FIG. 8: Comparisons between experimental level scheme of  $^{110}\text{Ru}$  [54] and TRM results with  $\gamma = 30^\circ$  and  $25^\circ$ . The excitation energies (in keV) and spin-parity values are given above the states. The widths and labels of the arrows represent the reduced  $E2$  transition probabilities in W.u.

energy spectra and electric quadrupole transition probabilities, wobbling motion in even-even nuclei could be

realized well for the states with small  $n$  phonon number when  $\gamma$  changing from  $\sim 25^\circ$  to  $\sim 35^\circ$ .

The above condition for the restriction of  $\gamma$  value is a relatively strict condition and might be difficult to achieve in realistic nuclei, which might be one of reasons for wobbling bands of purely collective were difficult to be observed in experiment. A recent data from coulomb excitation experiment, namely  $3_1^+$  and  $2_2^+$  for the  $^{110}\text{Ru}$  are studied and might be suggested as the bandhead of the candidate one- and two- phonon wobbling bands.

From azimuthal plot, the angular momentum geometry in the wobbling excitation has two types due to the different MoI: one is exhibited in the case of  $\gamma \sim 30^\circ$  and the other one in  $\gamma$  deviating from  $30^\circ$ . In a wobbling band with certain phonon number, the angle between an-

gular momentum and  $m$ -axis exhibits a decreasing trend with respect to spin.

### Acknowledgments

We are grateful to J. Meng and P. W. Zhao for helpful discussions. This work is supported in parts by National Natural Science Foundation of China (NSFC) under Grants No. 11675094 and 11622540, the Deutsche Forschungsgemeinschaft (DFG) and the NSFC through funds provided to the Sino-German CRC110 ‘‘Symmetries and the Emergence of Structure in QCD’’ (DFG Grant No. TRR110 and NSFC Grant No. 11621131001).

- 
- [1] S. Frauendorf, J. Meng, Nucl. Phys. A 617, 131 (1997).  
 [2] A. Bohr, B. R. Mottelson, Nuclear Structure, Vol. II, Benjamin, New York, 1975.  
 [3] S. Ødegård et al., Phys. Rev. Lett. 86, 5866 (2001).  
 [4] D. R. Jensen et al., Phys. Rev. Lett. 89, 142503 (2002).  
 [5] G. Schönwaßer et al., Phys. Lett. B 552, 9 (2003).  
 [6] H. Amro et al., Phys. Lett. B 553, 197 (2003).  
 [7] P. Bringel et al., Eur. Phys. J. A 24, 167 (2005).  
 [8] D. J. Hartley et al., Phys. Rev. C 80, 041304 (2009).  
 [9] J. T. Matta et al., Phys. Rev. Lett. 114, 082501 (2015).  
 [10] N. Sensharma et al., Phys. Lett. B 792, 170 (2019).  
 [11] S. Biswas et al., Eur. Phys. J. A 55, 159 (2019).  
 [12] J. Timár et al., Phys. Rev. Lett. 122, 062501 (2019).  
 [13] N. Sensharma et al., Phys. Rev. Lett. 124, 052501 (2020).  
 [14] S. Nandi et al., arXiv: nucl-ex, 2009.00493 (2020).  
 [15] S. Frauendorf, F. Dönau, Phys. Rev. C 89, 014322 (2014).  
 [16] I. Hamamoto, Phys. Rev. C 65, 044305 (2002).  
 [17] I. Hamamoto and B. R. Mottelson, Phys. Rev. C 68, 034312 (2003).  
 [18] G. B. Hagemann, Acta Phys. Pol. B 36, 4 (2005).  
 [19] E. Streck, Q. B. Chen, N. Kaiser, and Ulf-G. Meißner, Phys. Rev. C 98, 044314 (2018).  
 [20] K. Tanabe and K. Sugawara-Tanabe, Phys. Rev. C 95, 064315 (2017).  
 [21] R. Budaca, Phys. Rev. C 97, 024302 (2018).  
 [22] A. A. Raduta, R. Poenaru, and C. M. Raduta, Phys. Rev. C 101, 014302 (2020).  
 [23] M. Matsuzaki, et al., Phys. Rev. C 65, 041303(R) (2002).  
 [24] M. Matsuzaki, Y. R. Shimizu, and K. Matsuyanagi, Eur. Phys. J. A 20, 189 (2003).  
 [25] M. Matsuzaki and S.-I. Ohtsubo, Phys. Rev. C 69, 064317 (2004).  
 [26] M. Matsuzaki, Y. R. Shimizu, and K. Matsuyanagi, Phys. Rev. C 69, 034325 (2004).  
 [27] Y. R. Shimizu, M. Matsuzaki, and K. Matsuyanagi, Phys. Rev. C 72, 014306 (2005).  
 [28] Y. R. Shimizu, T. Shoji, and M. Matsuzaki, Phys. Rev. C 77, 024319 (2008).  
 [29] S. Frauendorf, F. Dönau, Phys. Rev. C 92, 064306 (2015).  
 [30] T. Nakatsukasa, K. Matsuyanagi, M. Matsuzaki, Y. R. Shimizu, Phys. Scr. 91, 073008 (2016).  
 [31] M. Shimada, Y. Fujioka, S. Tagami, and Y. R. Shimizu, Phys. Rev. C 97, 024318 (2018).  
 [32] Q. B. Chen, S. Q. Zhang, P. W. Zhao, and J. Meng, Phys. Rev. C 90, 044306 (2014).  
 [33] Q. B. Chen, S. Q. Zhang, and J. Meng, Phys. Rev. C 94, 054308 (2016).  
 [34] S. Frauendorf, Phys. Rev. C 97, 069801 (2018).  
 [35] K. Tanabe and K. Sugawara-Tanabe, Phys. Rev. C 97, 069802 (2018).  
 [36] E. A. Lawrie, O. Shirinda, and C. M. Petrache, Phys. Rev. C 101, 034306 (2020).  
 [37] I. N. Mikhailov and D. Janssen, Phys. Lett. 72B, 303 (1978).  
 [38] E. R. Marshalek, Nucl. Phys. A331, 429 (1979).  
 [39] Y. R. Shimizu and M. Matsuzaki, Nucl. Phys. A 588, 559 (1995).  
 [40] M. Oi, A. Ansari, T. Horibata, N. Onishi, Phys. Lett. B 480, 53 (2000).  
 [41] A. A. Raduta, R. Budaca, and C. M. Raduta, Phys. Rev. C 76, 064309 (2007).  
 [42] R. F. Casten, E. A. McCutchan, N. V. Zamfir, C. W. Beausang, and Jing-ye Zhang, Phys. Rev. C 67, 064306 (2003).  
 [43] W. X. Shi and Q. B. Chen, Chin. Phys. C 39, 054105 (2015).  
 [44] M. Oi, Physics of Atomic Nuclei 70, 1577 (2007).  
 [45] C. M. Petrache, P. M. Walker, S. Guo, Q. B. Chen, S. Frauendorf, Y. X. Liu, R. A. Wyss, D. Mengoni, Y. H. Qiang, A. Astier et al., Phys. Lett. B 795, 241 (2019).  
 [46] Q. B. Chen, et al., Phys. Rev. C 100, 061301(R) (2019).  
 [47] Y. K. Wang, F. Q. Chen and P. W. Zhao, Phys. Lett. B 802, 135246 (2020).  
 [48] J. H. Hamilton, et al., Nucl. Phys. A 834, 28c (2010).  
 [49] P. Ring and P. Schuck, The Nuclear Many-Body Problem, Springer, 1980.  
 [50] P. Möller, R. Bengtsson, B. G. Carlsson, P. Olivius, and T. Ichikawa, Phys. Rev. Lett. 97, 162502 (2006).  
 [51] F. Q. Chen, Q. B. Chen, Y. A. Luo, J. Meng, and S. Q. Zhang, Phys. Rev. C 96, 051303(R) (2017).  
 [52] Q. B. Chen and J. Meng, Phys. Rev. C 98, 031303(R) (2018).  
 [53] L. P. Gaffney et al., Nature 497, 199 (2013).  
 [54] D. T. Doherty, J. M. Allmond, R. V. F. Janssens et al., Phys. Lett. B 766, 334 (2017).